Journal of Atmospheric and Solar–Terrestrial Physics 156 (2017) 50–56

Contents lists available at ScienceDirect

Journal of Atmospheric and Solar–Terrestrial Physics

journal homepage: www.elsevier.com/locate/jastp

Terrestrial gamma-ray flashes in the BeppoSAX data archive

A. Ursi[a,b,*], C. Guidorzi[b], M. Marisaldi[c,d], D. Sarria[e], F. Frontera[b,d]

[a] INAF-IAPS, National Institute for Astrophysics, Roma, Italy
[b] Department of Physics and Earth Sciences, University of Ferrara, Ferrara, Italy
[c] Birkeland Centre for Space Science, University of Bergen, Norway
[d] INAF-IASF, National Institute for Astrophysics, Bologna, Italy
[e] CNRS, IRAP, Toulouse Cedex 4, France

ABSTRACT

Up to now, Terrestrial Gamma-ray Flashes (TGFs) have been mostly observed by instruments on-board satellites devoted to astrophysics: after the discovery by the BATSE/CGRO experiment in the early 90's, this elusive phenomenon has been further detected by RHESSI, by the AGILE satellite and by the Fermi space telescope. The Italian/Dutch satellite BeppoSAX (1996–2002) was one of the most important high-energy astrophysics missions, especially for what concerns the field of Gamma-Ray Bursts (GRBs). Its payload housed the Gamma-Ray Burst Monitor (GRBM), a segmented detector that could, in principle, have observed TGFs as well. Motivated by this possibility, we carried out, for the first time, a systematic search for TGFs in the BeppoSAX data archive, ending up with a sample of 12 TGF candidates. Among them, we also found a peculiar event, whose light curve characteristics may represent the signature of a mirrored Terrestrial Electron Beam (TEB).

1. Introduction

Terrestrial Gamma-ray Flashes (TGFs) are submillisecond intense gamma-ray (up to tens of MeV) emissions coming from the lowest part of the Earth's atmosphere, strictly correlated with thunderstorms. Unexpectedly discovered in 1994 by the Burst And Transients Source Experiment (BATSE) onboard the Compton Gamma-Ray Observatory (CGRO) (Fishman et al., 1994), TGFs have been successively observed by other satellites devoted to high-energy astrophysics, such as the Reuven Ramaty High-Energy Spectroscopic Imager (RHESSI) (Smith et al., 2005; Grefenstette et al., 2009), the Italian Astrorivelatore Gamma ad Immagini LEggero (AGILE) (Marisaldi et al., 2010, 2014) and the Fermi Space Telescope (Briggs et al., 2010). These bursts of gamma-rays are thought to be produced by electrons accelerated within thunderstorm electric fields, undergoing avalanche multiplication and successively braked, emitting high-energy photons via Bremsstrahlung (Dwyer, 2012; Xu et al., 2012; Celestin et al., 2012; Köhn et al., 2014; Köhn and Ebert, 2015). Feedback mechanisms involving X-rays and backscattered positrons may contribute to the process (Dwyer et al., 2003; Dwyer, 2008; Köhn et al., 2017).

Up to now, RHESSI (launched 2002) is considered the second satellite to observe TGFs, after the discovery by the BATSE/CGRO (operational between 1991 and 2000). However, in between these two missions, the BeppoSAX satellite (operational between 1996 and 2002) was fully operative and could, in principle, have detected TGFs as well. We investigate the historical BeppoSAX data archive, looking for signatures of TGFs, aimed at verifying whether its characteristics allowed for the detection of these terrestrial events as well.

2. The BeppoSAX satellite and the GRBM

The Satellite for X-ray Astronomy (SAX), renamed BeppoSAX after Giuseppe "Beppo Occhialini", was a project of the Italian Space Agency (ASI), with participation of the Netherlands Agency for Aerospace Programs (NIVR), that was operational from 1996 to 2002 (Piro, 1997). The spacecraft was launched in 1996 from Cape Canaveral Kennedy Space Center and delivered into a low-Earth 600 km altitude, 3.9° inclination orbit. It was successively dismissed and de-orbited in 2003, after 6 years successful activity.

BeppoSAX housed two classes of instruments, based on pointing direction and energy range. The first ones were the Narrow Field Instruments (NFIs), a set of different co-aligned instruments, consisting of four X-ray Low-Energy and Medium Energy Concentrator Spectrometers (LECS and MECS), a High Pressure Gas Scintillation Proportional Counter (HPGSPC) and a Phoswich Detection System (PDS), ensuring an energy coverage from 0.1 to 300 keV. The second

* Corresponding author at: INAF-IAPS Roma, Via Fosso del Cavaliere 100, I-00133 Roma, Italy.
E-mail address: alessandro.ursi@iaps.inaf.it (A. Ursi).

http://dx.doi.org/10.1016/j.jastp.2017.02.014
Received 23 January 2017; Received in revised form 24 February 2017; Accepted 26 February 2017
Available online 02 March 2017
1364-6826/

class of instruments was the Wide Field Cameras (WFCs), a set of two co-aligned coded masks, with a 20°·20° FOV, sensitive in the range 1.8 − 28 keV.

The PDS was surrounded by four CsI(Tl) scintillators slabs, composing the Gamma-Ray Burst Monitor (GRBM): this squared detector was initially thought as an anticoincidence module and later turned into an all-sky monitor for gamma-ray sources (Frontera et al., 1997). Each GRBM panel had a 1136 cm^2 geometrical area and a wide energetic coverage, from 40 keV up to 700 keV. The GRBM did not have imaging capabilities and only allowed for a rough reconstruction of the incoming direction of the detected events, with an accuracy of about 15° − 40° (Frontera et al., 2009).

One-second resolution data were continuously acquired in two energy channels: the GRBM band (40 − 700 keV) and the Anti-Coincidence (AC) band (≥100 keV). High time resolution (HTR) data in the first band were acquired whenever a trigger was issued on-board: this occurred whenever an excess of counts over the background rate was detected, in at least two units out of four. HTR data have a resolution of 7.8125 ms(=1 *s*/128). Data acquisition started whenever the deposited counts exceeded a threshold, settable to 4σ, 8σ, or 16σ, depending on a dynamic average background rate, evaluated on both Long (8 − 128 s) and Short (~7.8 ms) Integration Time intervals (LIT/SIT). A typical GRBM trigger acquisition consists of a 106 s time window, starting from t_0 − 8 s and lasting to t_0 + 98 s , with t_0 time at which the trigger was issued. The 10 s following the t_0 are available also with a higher time resolution of ~0.48 ms(=7.8125 ms/16).

3. Search for TGFs

The quest of TGFs was carried out in two steps: first, we performed simulations of typical TGFs, convolved with the GRBM response matrix for a number of possible different directions with respect to the payload reference frame, in order to understand what a typical event would look like, if detected by the instrument. On the basis of this result, we developed a dedicated search algorithm, aimed at finding the expected events in the whole GRBM database.

3.1. The GRBM as a TGF detector

From an accurate overview of the GRBM main technical characteristics, three major drawbacks concerning TGF detection may be pointed out: such issues are all ascribed to the instrument coarse time resolution and represent basic limitation to our analysis.

First, the integration times upon which the on-board trigger condition is set are generally too long (7.8 ms–4 s) to be sensitive to the shortness of TGFs: such an effect was already observed in the GRB catalog, in terms of the relatively few short GRBs detected with the GRBM, compared with the BATSE catalogs. Since typical TGFs would not release a large amount of counts in the detector, as shown in Table 1, we expect that such events would not trigger the GRBM and should be searched into the available total trigger dataset. Simulations of typical TGFs, convolved with the GRBM response matrix, provide information about the total number of counts deposited by a standard TGF in every detector unit. We adopted the empirical TGF spectrum developed by Dwyer and Smith (2005), based on the best fit to RHESSI data and corresponding to a production height of 15–21 km, and a set of various incoming angles with respect to the payload frame: zenith angles in range [n·15°, with n = (0 − 12)] and azimuth angles in range [m·45°, with m = (0 − 8)]. Results from simulations are shown in Table 1, where the number of counts expected in each GRBM unit is presented, together with the corresponding value of fluence (expressed as photons / cm^2) and the expected mean occurrence rate dN/dt of such events: a typical RHESSI TGF with 0.1 ph cm^{-2} fluence in the 1 keV–20 MeV energy range would release ~10 counts in each GRBM unit. Given typical background rates, events with higher fluences would release a higher number of counts, but are less frequent, as the fluence distribution decreases as a cut-off index power law with spectral index $\alpha = -2.3$ (Ostgaard et al., 2012; Tierney et al., 2013; Marisaldi et al., 2014).

Table 1
Number of counts N_{exp} expected in each single GRBM unit, from typical TGFs with different values of fluence $F = N_\gamma/A_{eff}$ [photons / cm^2]: the corresponding expected mean rate dN/dt of such events, as obtained by simulations, is shown in the second column.

F [ph·cm^{-2}]	dN/dt [day^{-1}]	N_{exp} in 1 unit
0.1	0.20	≤11
0.2	0.08	≤21
0.3	0.04	≤30
0.4	0.03	≤40
0.5	0.02	≤52

Second, the 7.8 ms time resolution available for each trigger is much longer than the typical 0.1 ms TGF duration: in this case, all counts due to a single burst would be entirely smeared onto a single 7.8 ms bin, not providing information about the time profile of the event and making the related light curve appear just as a sharp spike above the background. The 0.5 ms high time resolution may be more useful, especially if dealing with longer duration TGFs, but it is available for a shorter period of time (only 10 s for each trigger). Unfortunately, longer lasting TGFs may occur, but are rare: according to the AGILE sample detected with the new enhanced configuration (Marisaldi et al., 2015), about 25% of the detected TGFs show durations longer than 500 μs.

Third, the only other available energy channel (AC band) provides data with a 1 s time resolution, which is useless for TGF analysis: the absence of more than one useful energy channel prevents any kind of spectral study.

On the other hand, the BeppoSAX 3.9° inclination orbit may play a role in the detection of TGFs, compared to the 28.5° inclination orbit of the CGRO, making the GRBM scan a narrower equatorial strip, with a higher TGF occurrence rate density. Taking into consideration RHESSI, that has the highest inclination orbit among the satellites observing TGFs, the detection rate density within ±5° (consistent with the region scanned by BeppoSAX) is about 2 times the detection rate density within ±40° (consistent with the RHESSI nominal orbit inclination), putting the GRBM in a slightly more favorable condition for the observation of TGFs.

The most important result that can be derived from these simulations is that typical TGFs could not trigger the GRBM onboard logic, as shown in Fig. 1. As a consequence, the search for TGFs was carried out by considering the whole dataset of triggers, during which the detector was active and acquiring HR data. In 6 years activity, from July 6th, 1996 to April 27th, 2002, the GRBM was triggered 19216 times by high-energy transients (such as gamma-ray bursts, soft gamma-ray repeaters, solar flares), as well as by spurious events (such as occultation steps of known high-energy sources, pre-South Atlantic Anomaly (SAA) events and background high-energy charged particles, strong enough to release counts into more than one GRBM unit) accounting for an exposure time of ~24 days.

The geographic distribution is an important check for the goodness of a TGF candidate sample, but it can be considered reliable only if all the issued triggers do not already exhibit some longitude or latitude preferred pattern, except for local enhancements in the proximity of the SAA region. Tests show that the triggers are uniformly distributed throughout Earth's surface, not exhibiting privileged geographic regions of occurrence.

3.2. Search algorithm and expected number of events

The typical background rate in each single unit of the GRBM is about 5–8 cts /7.8 ms (with a slightly higher rate for the second unit, parallel to the solar panels and facing the Sun): it consists of a diffuse

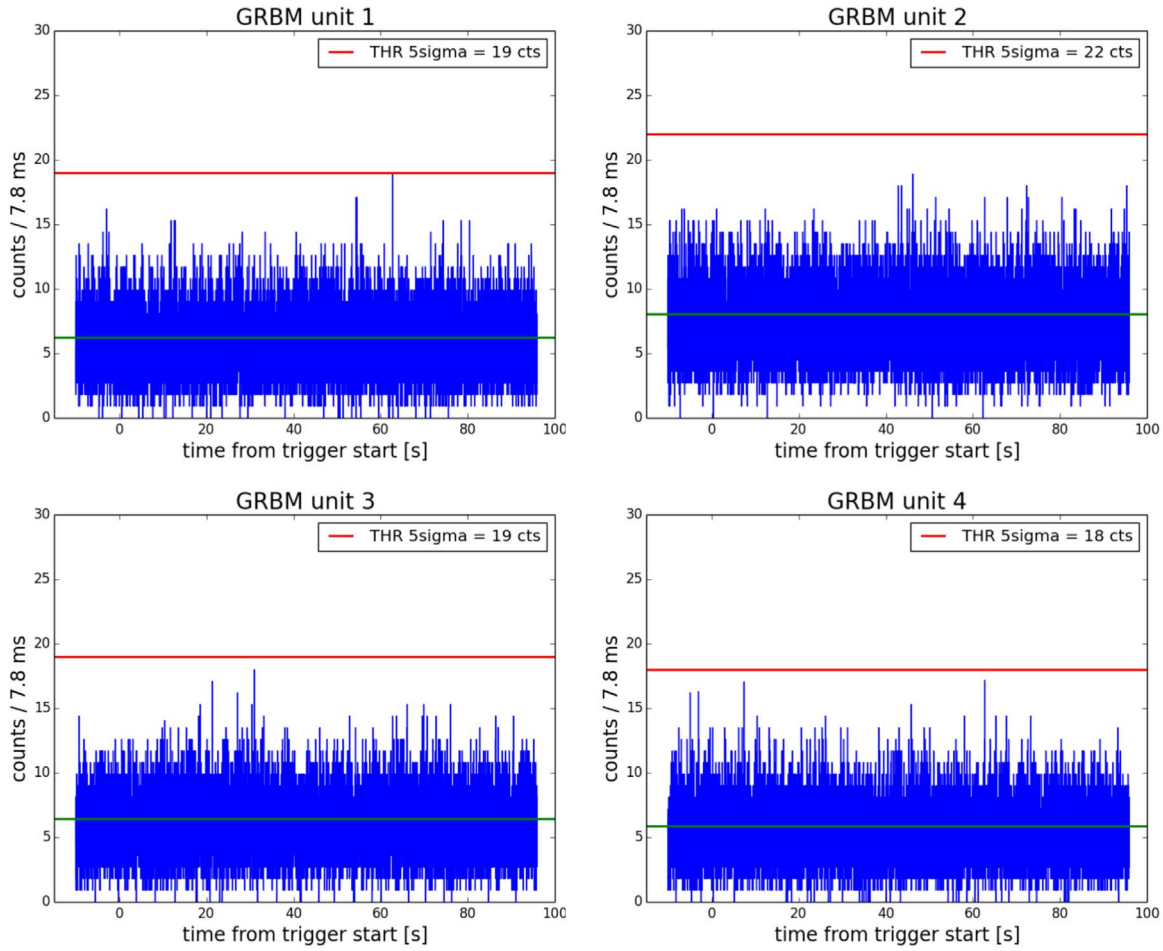

Fig. 1. Typical trigger acquisition of the GRBM, in the 7.8 ms timescale. For each unit, the background rate (green line) and the corresponding 5σ threshold count rate (red line) are shown: it is evident that, according to Table 1, TGFs with fluences $F \leq 0.2$ ph·cm^{-2} and $N_{exp} \leq 21$ are not expected to likely release a sufficient number of counts, in each unit, to overcome a 5σ threshold level. (For interpretation of the references to color in this figure legend, the reader is referred to the web version of this article.)

X- and gamma-ray noise, cosmic rays and other high-energy charged particles, inducing fluorescent signatures in the detector, as well as pre-SAA events and other known X- and gamma-ray cosmic sources. Typical TGFs with 0.1 ph cm^{-2}, releasing ~10 counts in a single bin, in each unit, are easily confused in the background and should be therefore distinguished by exploiting the segmented nature of the detector, as shown in Fig. 1. As a consequence, events with higher fluence are easier to be discriminated, though they are rarer.

The background rate μ has been calculated as the mean count rate per bin within each 106 s entire trigger window, individually, for each trigger acquisition. We obtain a mean rate of $\mu = 5 - 8$ cts/bin, corresponding to $600 - 900$ Hz, for each GRBM unit. A chi-squared test is performed at the same time, to check whether the calculated background follows a Poisson distribution: all trigger acquisition whose background does not follow a Poisson distribution within 90% confidence are rejected, as they are affected by some long-lasting gamma-ray event, that prevents the identification of faint spikes in the lightcurve.

The cumulative probability to obtain a number of counts equal or greater than N, released within a single bin, for a count rate following a Poisson distribution with mean value μ, is equal to:

$$p(n \geq N)\Big|_{\mu} = 1 - \sum_{m=0}^{N-1} \mu^m \frac{e^{-\mu}}{m!} \tag{1}$$

where we assume a distribution normalized to 1. Given a certain average background rate μ in a single GRBM unit, we can select the threshold N, needed to have a total probability, calculated over all the bins of a single 106 s long light curve, less than a $p_{5\sigma} = 5.73 \cdot 10^{-7}$, corresponding to a 5σ confidence level. A typical background rate of $\mu = 6$ cts/bin requires a threshold of N=22 cts: however, simulation show that this is too high to be achieved by a typical TGF, in a single GRBM unit.

The search algorithm investigates the electromagnetic nature of the event, by looking whether the TGF is detected simultaneously in at least three units out of four. Events observed in less than three units are difficult to be distinguished from background fluctuations or electronic noise inside the detector, that may affect just parts of the whole instrument, and are therefore rejected. If we assume that the spike produced by the TGF is observed in at least k units out of four, simultaneously, the total probability will be equal to:

$$P(k) = N_{bin} \sum_{i=0}^{k} \binom{4}{i} p^i (1-p)^{4-i} \tag{2}$$

for a number of $N_{bin} = 13568$ independent trials, corresponding to the total number of 7.8 ms bins within a 106 s trigger window. Considering k=4 and k=3, this reduces to:

$$\begin{cases} k = 4 & P = N_{bin} p^4 \\ k = 3 & P = N_{bin}(4p^3 - 3p^4) \end{cases} \tag{3}$$

This method allows to obtain a good handle on the rejection of statistical fluctuations and charged particles, by imposing looser constraints on each unit. Requiring the global probability for a spike to occur within the same time bin in four or three units to be $P_{5\sigma} = 5.7 \cdot 10^{-7}$, as of Eq. (1) translates into a required probability in

each independent GRBM unit:

$$\begin{cases} P_{5\sigma} = 5.7\cdot10^{-7} = N_{bin}p_{5\sigma_4}^4 & \text{with } p_{5\sigma_4} = 2.5\cdot10^{-3} \\ P_{5\sigma} = 5.7\cdot10^{-7} = N_{bin}(4p_{5\sigma_3}^3 - 3p_{5\sigma_3}^4) & \text{with } p_{5\sigma_3} = 2.1\cdot10^{-4} \end{cases} \quad (4)$$

where we adopt the notation nσ_k to identify a selection criterion selecting events with a global confidence level of $P_{n\sigma}$ and detected in at least k GRBM units out of four. The same line of reasoning can be applied also to a global probability of $P_{4\sigma} = 4.6\cdot10^{-6}$: requiring the global probability for a spike to occur within the same time bin in four or three units to be $P_{4\sigma}$, the corresponding required probability in each independent GRBM unit will be equal to:

$$\begin{cases} P_{4\sigma} = 4.6\cdot10^{-6} = N_{bin}p_{4\sigma_4}^4 & \text{with } p_{4\sigma_4} = 4.3\cdot10^{-3} \\ P_{4\sigma} = 4.6\cdot10^{-6} = N_{bin}(4p_{4\sigma_3}^3 - 3p_{4\sigma_3}^4) & \text{with } p_{4\sigma_3} = 4.4\cdot10^{-4} \end{cases} \quad (5)$$

Moreover, adopting these thresholds, a negligible number of false positives is expected over the entire data sample covering 6 years (19216 triggers): $P_{5\sigma}$ and $P_{4\sigma}$ probabilities, that refer to a single light curve, produce a total number of false positives equal to $19216\cdot P_{5\sigma} \sim 0.01$ and $19216\cdot P_{4\sigma} \sim 0.1$, respectively, when considering the total number of triggers.

For the typical background rate $\mu = 6$ cts/bin discussed before, a number of $N_i \geq 15$ cts should be deposited in each detector unit simultaneously, in order to be within a 5σ confidence level, which is a much more achievable number of counts for a typical TGF. As an illustrative example, in Fig. 2 the four lightcurves of the GRBM units are shown, together with the mean background rate and the required 5σ threshold, for (a) an event selected by the algorithm and later classified as TGF candidate 990504 and (b) an event that did not trigger the algorithm. In the first case, a spike exceeding the required threshold occurs in all four detector units, within the same 7.8 ms time bin, while in the second case, a spike is observed in just two units out of four, not triggering the search algorithm.

It is useful to predict how many TGFs should have been observed in 6 years activity by BeppoSAX. This number basically depends on the effective exposure during the whole mission and the detector sensitivity to events. The effective exposure of the satellite is the total time during which the detector was active and acquiring HR data. According to the selection algorithm, the minimum number of counts required to identify a candidate TGF with a 5σ confidence level is equal to about ~17 cts in at least three units out of four, over a typical background rate of 6 cts/7.8 ms, corresponding to a total number of 51 cts. Considering an effective area of about 300 cm^2 at $E \geq 600$ keV, a minimum detectable fluence of $F_{min} \sim 0.2$ ph cm^{-2} is obtained: this is consistent with results from simulations presented in Table 1. As the expected number of TGFs with a given fluence is described by a simple power law with spectral index $\alpha = -2.3$ (Ostgaard et al., 2012), the minimum TGF detection rate expected for the GRBM is equal to 0.1 TGFs / day. Taking into consideration 24 days of exposure, a total number of 2–3 TGFs is expected to be detected in 6 years activity. It is worth noticing that this is a rough estimate, as the background rate strongly varies throughout the entire mission, as well as the minimum detectable fluence and the corresponding expected number of events.

4. Results and discussion

The search for TGFs ended up with 12 candidates, listed in Table 2 and geographically shown in Fig. 3. The last four columns of Table 2 display the different adopted selection criteria: $5\sigma_4$, $5\sigma_3$, $4\sigma_4$ and $4\sigma_3$. It is worth noticing that events fulfilling the $5\sigma_4$ condition automatically fulfill the $4\sigma_4$ condition, as well as that events fulfilling the $5\sigma_3$ condition automatically fulfill the $4\sigma_3$ condition. This is the case when confidence levels refer to the same number of units: this ensures that the 5σ accuracy is higher than the 4σ. As a consequence, 5 of the 6 TGF candidates satisfying the $4\sigma_4$ condition do also satisfy the $5\sigma_4$ condition, while 7 of the 12 TGF candidates fulfilling the $4\sigma_3$ criterion also fulfill the $5\sigma_3$. However, it does not imply that an event satisfying the $5\sigma_4$ condition also satisfies the $5\sigma_3$ condition, as a different number of units is considered and the corresponding confidence level change (the $5\sigma_3$ criterion requires a slightly higher number of counts in each unit with respect to the $5\sigma_4$ criterion). A further search, carried out by imposing $3\sigma_4$ and $3\sigma_3$ threshold levels, produced >1200 candidates, that exhibit an evident uniform geographic distribution, with no clustering over the most thunderstorm active regions: such fake candidates are mostly ascribed to electronic noise and other spurious signals and have been therefore rejected.

Although the sample is quite limited, it exhibits an evident clustering over the continental regions, reflecting the common behavior of a genuine TGF geographic distribution, with 3 events occurring over Africa, 8 over the maritime continent and only 1 over the Pacific Ocean. All events show expected time profiles integrated within a single 7.8 ms time bin, appearing as spikes above the background. The total number of counts released by these candidates, summed over all of the four detectors, ranges from a minimum of 56 cts, in conditions of particularly favorable low background rate, to a maximum of 100 cts, for the strongest case (not considering event TGF000308, that will be discussed in detail later in this Section). The ratio of counts deposited among the GRBM units can be used to roughly estimate the incoming direction of the detected event: the spatial resolution of this reconstruction is quite coarse, but sufficient to understand whether the more exposed units were facing the Earth or not, by taking into consideration the spacecraft configuration at the time the event was detected. Except for TGF000308, all candidates exhibit count ratios consistent with an incoming terrestrial direction, within $20^\circ - 40^\circ$ uncertainty.

Candidate TGF000308, taking place in central Africa, shows an interesting time profile, with two pulses 46 ms apart, as shown in Fig. 4(a). Differently from the other TGF candidates, this event produced a large number of total counts (up to ~495 cts) within the same 7.8 ms time bin. In this case, the ratio of counts among the GRBM units shows that the two pulses have opposite incoming directions, with the first stronger peak compatible with a sky origin and the second fainter peak compatible with a terrestrial origin. Given the huge number of counts, the first spike of TGF000308 was the only candidate able to trigger the onboard GRBM logic: as a consequence, data in both 7.8 ms (blue line) and 0.5 ms (red line) time resolution are available for the second pulse, providing more detailed information. This smaller pulse exhibits a fast rise and exponential decay time profile, with a total duration of about 4 – 5 ms, which is rather large compared to TGF typical durations. Considering the large number of counts released in the detector, the different incoming direction and intensity of the two pulses and the time profile of the second peak, we suggest this could be the signature of an electron TGF or Terrestrial Electron Beam (TEB), that propagates along the geomagnetic field line towards the opposite hemisphere and is mirrored back to the satellite after interaction with the atmosphere; in addition, this area over central Africa is known to already have hosted this kind of events (such as the Fermi 091214 event (Briggs et al., 2011)). Instruments revealing TGFs, such as BATSE, RHESSI and Fermi, do also detect TEBs, as reported in (Dwyer, 2008; Briggs et al., 2011). The bunches of electrons (and possibly positrons) constituting TEBs can travel very long distances along the geomagnetic field lines before being detected, with an originating storm placed thousand of kilometers away from the subsatellite point. Although exhibiting longer (~ms) durations with respect to typical TGFs, these beams would appear just like normal TGFs for a detector like the GRBM and would be integrated within the same 7.8 ms time bin. Simulations of a TEB, detected at the satellite altitude at the time of the event, have been carried out, by using the MC-PEPTITA Monte Carlo model (Sarria et al., 2015). We assumed a TGF source located at about longitude =35.5° and latitude =−9.5°, and a TGF producing the electron beam placed at ~13 km altitude, so that the produced TEB reaches 574 km altitude approximately at the

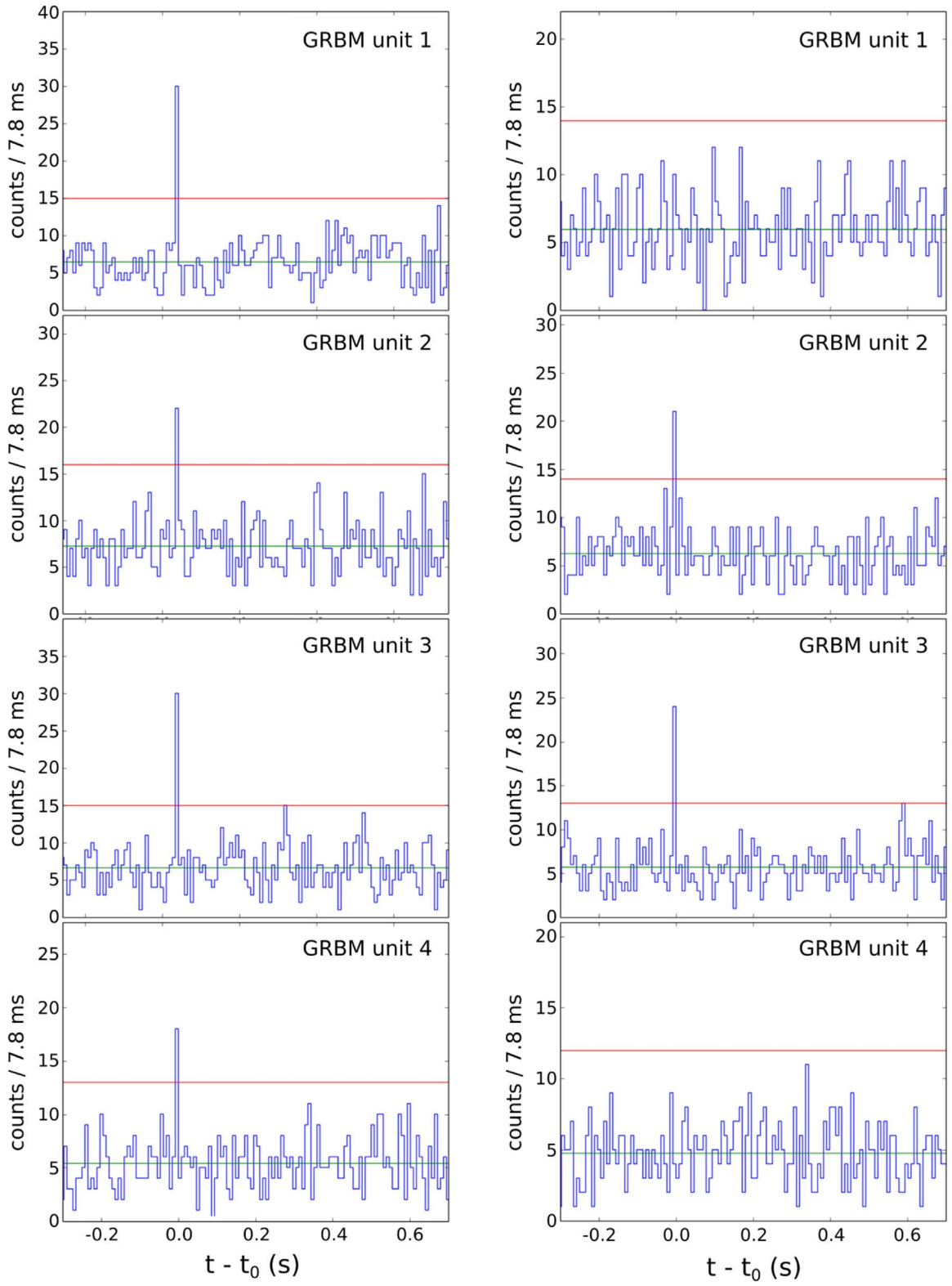

Fig. 2. Working principle of the TGF search algorithm, for the $5\sigma_4$ selection criterion. Panel (a) shows a spike exceeding the required thresholds (red lines) above the mean background rates (green lines) in each GRBM unit simultaneously, needed to obtain a total 5σ confidence level and select the event as a possible TGF candidate. Panel (b) exhibits the same principle for another event, whose condition is satisfied in only two GRBM units out of four, and therefore is not selected as a possible TGF candidate.(For interpretation of the references to color in this figure legend, the reader is referred to the web version of this article.)

coordinates of BeppoSax, at the time it detected the event (longitude =35.31°, latitude =−3.17°). The simulation represented in Fig. 4(b) shows that an electron TGF coming from the south and mirrored back along the same geomagnetic field line would produce two pulses, with different intensities. The relative magnitude between the main pulse (5–20 ms) and the mirror pulse (58 – 65 ms) is accurately reproduced by the model. However, the time delay between the two peaks is about 15% longer in the simulation, with respect to the observation. The

Table 2
The 12 TGF candidates obtained by the search algorithm.

ID	lon [deg]	lat [deg]	date	time [UT]	N_{cts}	$5\sigma_4$	$5\sigma_3$	$4\sigma_4$	$4\sigma_3$
971215	112.09	−0.83	1997–12–15	15:15:14	76	✓	✓		✓
981128	101.94	3.73	1998–11–28	22:51:21	97		✓	✓	✓
990504	113.90	3.94	1999–05–04	06:04:42	100	✓	✓	✓	✓
000308	35.31	−3.17	2000–03–08	20:20:16	140	✓	✓	✓	✓
001002	103.08	3.72	2000–10–02	00:59:35	65				✓
001003	146.02	−2.17	2000–10–03	17:13:34	78	✓	✓	✓	✓
001119	31.49	−1.54	2000–11–19	22:55:57	70	✓	✓	✓	✓
010807	−136.06	1.34	2001–08–07	08:04:11	57				✓
011231	29.84	−2.25	2001–12–31	06:18:19	78			✓	✓
020302	124.84	−3.96	2002–03–02	08:35:25	56				✓
020304	105.15	−3.71	2002–03–04	07:31:19	63			✓	✓
020328	100.26	−3.38	2002–03–28	17:03:21	57				✓

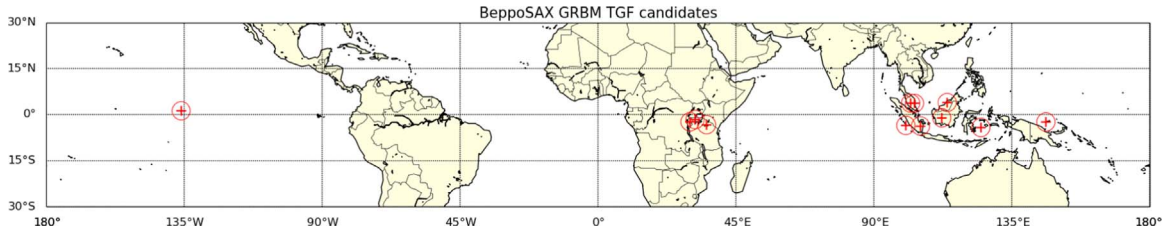

Fig. 3. Geographic distribution of the 12 TGF candidates satisfying the threshold criterion imposed by our search algorithm. Red circled crosses correspond to the satellite footprint at the TGF time, with associated 6°-diameter uncertainty regions. Although the sample is small, events seem to follow the typical TGF geographic distribution, clustering over central Africa and over the maritime continent. (For interpretation of the references to color in this figure legend, the reader is referred to the web version of this article.)

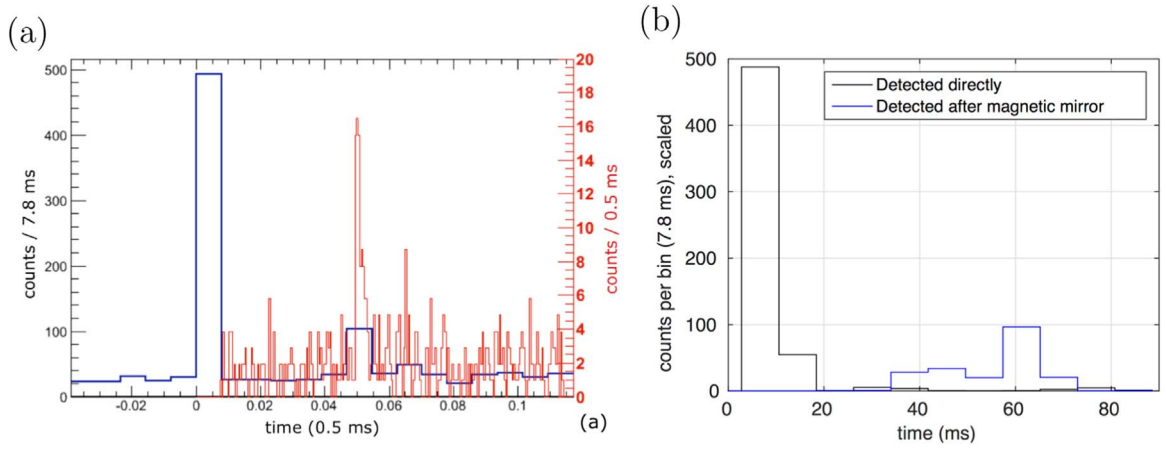

Fig. 4. (a) Light curve of TGF candidate 000308, suspected to be a mirrored electron TGF, plotted both with 7.8 ms (blue) and 0.5 ms (red) timescales. (b) Simulation of a TEB, taking place in the south and detected at the same time and altitude of BeppoSAX, taking into account the related geomagnetic field, turns out to be consistent within 15%. (For interpretation of the references to color in this figure legend, the reader is referred to the web version of this article.)

accuracy of the integrator used to compute the motion of the electrons in the geomagnetic field was carefully checked and did not show any problem and this difference could therefore rely in local inaccuracies in the used International Geomagnetic Reference Field (IGRF) model (Finlay et al., 2010).

The probability that this event could be the result of an electron TGF is further underlined by the associated reconstructed meteorological images, shown in Fig. 5: the 11 μm brightness temperature, typically associated to the cloud top temperature, acquired by the Meteosat First Generation (MFG) Meteosat-7 satellite on March 3rd, 2000 at UTC 20:15:00 (i.e., about only five minutes before the TGF time), shows the presence of an intense and extended convective system in the region compatible with the electron TGF source adopted for the simulation, whereas within a 6° radius uncertainty circle around the satellite footprint no significant convection is observed.

5. Conclusions

The BeppoSAX satellite was one of the most important missions in the field of high-energy astrophysics, endowed with instruments similar to those carried by BATSE on-board the CGRO, that detected 79 TGFs between 1991 and 2000. Motivated by the possibility that the BeppoSAX GRBM detected TGFs as well, we developed a search algorithm to find very short and faint events, inside the GRBM data archive, by exploting the segmented nature of the detector. The low time resolution and the low sensitivity to the typical TGF fluences severely hampered this search; also, the absence of useful spectral data prevented any kind of spectral analysis on the sample events. Nevertheless, we ended up with a sample of 12 TGF candidates, that cannot be solidly confirmed as TGFs, but that satisfy some basic expected requirements: first, the candidates geographic distribution is consistent with a typical TGF population, clustering over the land, especially in Africa and in the maritime continent. Second, the number of candidates is also consistent with the expected number of TGFs

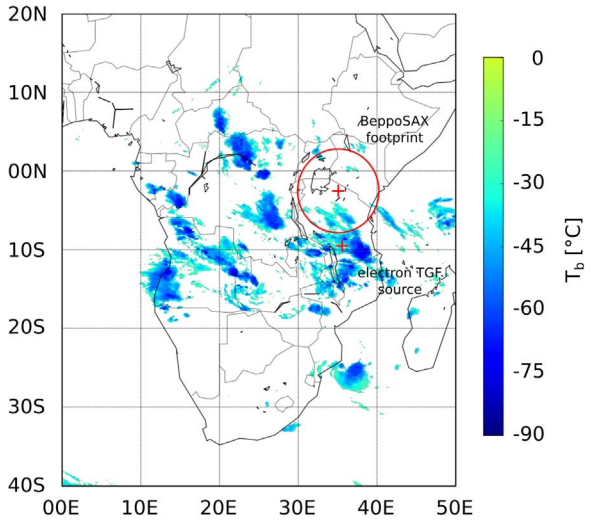

Fig. 5. Meteorological scenario associated to the BeppoSAX TGF000308, suspected to be a mirrored TEB, reconstructed by means of the Meteosat-7 11 μm brightness temperature, on March 3rd, 2000 at UTC 20:15:00. The red cross represents the satellite footprint at the detection time: the 6° radius uncertainty circle surrounding this point shows no significant presence of convective systems. On the contrary, the green cross, which represents the region compatible with the simulated beam source, lies within a strong and extended convective context, suggesting the TGF could have originated in the southern point and have been detected in the northern point after propagation along the geomagnetic field line. (For interpretation of the references to color in this figure legend, the reader is referred to the web version of this article.)

detected by the GRBM in six years activity, taking into account the exposure time, the geographic region scanned by the satellite and the sensitivity of the detector. Finally, the rough reconstruction of the incoming direction for each of these events, based on the evaluation of the ratio of counts among the different GRBM units, is always consistent with a terrestrial origin. Unexpectedly, among these candidate TGFs, we identified a peculiar event occurring over Africa, exhibiting a double pulse in the light curve, with a first stronger peak consistent with a sky incoming direction and a second fainter peak consistent with a terrestrial incoming direction: simulations by means of the geomagnetic field lines at the time of the event and at the altitude at which it was detected by BeppoSAX show that this could be the signature of a mirrored electron TGF over Africa, produced in the southern region of the continent and bounced back in the northern part. This study represents the first probable evidence of a fifth high-energy astrophysics mission capable of detecting TGFs, as well as TEBs, filling the gap between the first detections by BATSE and the successive events recorded by RHESSI. Although BeppoSAX is no longer operative, the statistical analysis developed for this study could be exploited for next generation instruments dedicated to TGF research, such as ASIM and TARANIS.

References

Briggs, M.S., et al., 2010. First results on terrestrial gamma ray flashes from the Fermi Gamma-ray Burst Monitor. J. Geophys. Res. (Space Phys.) 115, A07323. http://dx.doi.org/10.1029/2009JA015242.

Briggs, M.S., Connaughton, V., Wilson-Hodge, C., Preece, R.D., Fishman, G.J., Kippen, R.M., Bhat, P.N., Paciesas, W.S., Chaplin, V.L., Meegan, C.A., von Kienlin, A., Greiner, J., Dwyer, J.R., Smith, D.M., 2011. Electron-positron beams from terrestrial lightning observed with Fermi GBM. Geophys. Res. Lett. 38, L02808. http://dx.doi.org/10.1029/2010GL046259.

Celestin, S., Xu, W., Pasko, V.P., 2012. Terrestrial gamma ray flashes with energies up to 100 MeV produced by nonequilibrium acceleration of electrons in lightning. J. Geophys. Res. (Space Phys.) 117, A05315. http://dx.doi.org/10.1029/2012JA017535.

Dwyer, J.R., Uman, M.A., Rassoul, H.K., Al-Dayeh, M., Caraway, L., Jerauld, J., Rakov, V.A., Jordan, D.M., Rambo, K.J., Corbin, V., Wright, B., 2003. Energetic radiation produced during rocket-triggered lightning. Science 299, 694–697. http://dx.doi.org/10.1126/science.1078940.

Dwyer, J.R., 2008. Source mechanisms of terrestrial gamma-ray flashes. J. Geophys. Res. 113, D10103. http://dx.doi.org/10.1029/2007JD009248.

Dwyer, J.R., 2012. The relativistic feedback discharge model of terrestrial gamma ray flashes. J. Geophys. Res. (Space Phys.) 117, A02308. http://dx.doi.org/10.1029/2011JA017160.

Dwyer, J.R., Smith, D.M., 2005. A comparison between Monte Carlo simulations of runaway breakdown and terrestrial gamma-ray flash observations. Geophys. Res. Lett. 22 (32). http://dx.doi.org/10.1029/2005GL023848, 804–+.

Finlay, C.C., Maus, S., Beggan, C.D., Bondar, T.N., Chambodut, A., Chernova, T.A., Chulliat, A., Golovkov, V.P., Hamilton, B., Hamoudi, M., Holme, R., Hulot, G., Kuang, W., Langlais, B., Lesur, V., Lowes, F.J., Lühr, H., MacMillan, S., Mandea, M., McLean, S., Manoj, C., Menvielle, M., Michaelis, I., Olsen, N., Rauberg, J., Rother, M., Sabaka, T.J., Tangborn, A., Tøffner-Clausen, L., Thébault, E., Thomson, A.W.P., Wardinski, I., Wei, Z., Zvereva, T.I., 2010. International geomagnetic reference field: the eleventh generation. Geophys. J. Int. 183, 1216–1230. http://dx.doi.org/10.1111/j.1365-246X.2010.04804.x.

Fishman, G.J., et al., 1994. Discovery of intense gamma-ray flashes of atmospheric origin. Science 264, 1313–1316.

Frontera, F., et al., 1997. PDS experiment on board the BeppoSAX satellite: design and in-flight performance results. EUV, X-Ray Gamma-Ray Instrum. Astron. VIII 3114, 206–215.

Frontera, F., Guidorzi, C., Montanari, E., Rossi, F., Costa, E., Feroci, M., Calura, F., Rapisarda, M., Amati, L., Carturan, D., Cinti, M.R., Fiume, D.D., Nicastro, L., Orlandini, M., 2009. The gamma-ray burst catalog obtained with the gamma-ray burst monitor aboard BeppoSAX. Astrophys. J. Suppl. 180, 192–223. http://dx.doi.org/10.1088/0067-0049/180/1/192.

Grefenstette, B.W., Smith, D.M., Hazelton, B.J., Lopez, L.I., 2009. First RHESSI terrestrial gamma ray flash catalog. J. Geophys. Res. 114, A02314. http://dx.doi.org/10.1029/2008JA013721.

Köhn, C., Ebert, U., Mangiarotti, A., 2014. The importance of electron-electron bremsstrahlung for terrestrial gamma-ray flashes, electron beams and electron-positron beams. J. Phys. D. Appl. Phys. 47 (25), 252001. http://dx.doi.org/10.1088/0022-3727/47/25/252001.

Köhn, C., Ebert, U., 2015. Calculation of beams of positrons, neutrons, and protons associated with terrestrial gamma ray flashes. J. Geophys. Res. (Atmospheres) 120, 1620–1635. http://dx.doi.org/10.1002/2014JD022229.

Köhn, C., Diniz, G., Harakeh, M.N., 2017. Production mechanisms of leptons, photons, and hadrons and their possible feedback close to lightning leaders. J. Geophys. Res.: Atmos. 122 (2), 1365–1383. http://dx.doi.org/10.1002/2016JD025445, (2016JD025445).

Marisaldi, M., et al., 2010. Detection of terrestrial gamma ray flashes up to 40 MeV by the AGILE satellite. J. Geophys. Res. (Space Phys.) 115, A00E13. http://dx.doi.org/10.1029/2009JA014502.

Marisaldi, M., et al. 2014. The first AGILE low-energy (<30 MeV) Terrestrial Gamma-ray Flashes catalog. In EGU General Assembly Conference Abstracts. EGU General Assembly Conference Abstracts, vol. 16, p. 11326.

Marisaldi, M., Argan, A., Ursi, A., Gjesteland, T., Fuschino, F., Labanti, C., Galli, M., Tavani, M., Pittori, C., Verrecchia, F., D'Amico, F., Østgaard, N., Mereghetti, S., Campana, R., Cattaneo, P.W., Bulgarelli, A., Colafrancesco, S., Dietrich, S., Longo, F., Gianotti, F., Giommi, P., Rappoldi, A., Trifoglio, M., Trois, A., 2015. Enhanced detection of terrestrial gamma-ray flashes by AGILE. Geophys. Res. Lett. 42, 9481–9487. http://dx.doi.org/10.1002/2015GL066100.

Ostgaard, N., et al., 2012. The true fluence distribution of terrestrial gamma flashes at satellite altitude. J. Geophys. Res. (Space Phys.) 117, A03327. http://dx.doi.org/10.1029/2011JA017365.

Piro, L., 1997. BeppoSAX overview. In: Proceedings of the Fourth Compton Symposium, American Institute of Physics Conference Series, vol. 410, edited by Dermer, C.D., Strickman, M.S., Kurfess, J.D. pp. 1485–1492http://dx.doi.org/10.1063/1.53959.

Sarria, D., Blelly, P.-L., Forme, F., 2015. Mc-peptita: a monte carlo model for photon, electron and positron tracking in terrestrial atmosphere. application for a terrestrial gamma-ray flash. J. Geophys. Res.: Space Phys.. http://dx.doi.org/10.1002/2014JA020695, (pp. n/a–n/a, 2014JA020695).

Smith, D.M., et al., 2005. Terrestrial gamma-ray flashes observed up to 20 MeV. Science 307, 1085–1088.

Tierney, D., Briggs, M.S., Fitzpatrick, G., Chaplin, V.L., Foley, S., McBreen, S., Connaughton, V., Xiong, S., Byrne, D., Carr, M., Bhat, P.N., Fishman, G.J., Greiner, J., Kippen, R.M., Meegan, C.A., Paciesas, W.S., Preece, R.D., Kienlin, A., Wilson-Hodge, C., 2013. Fluence distribution of terrestrial gamma ray flashes observed by the Fermi Gamma-ray Burst Monitor. J. Geophys. Res. (Space Phys.) 118, 6644–6650. http://dx.doi.org/10.1002/jgra.50580.

Xu, W., Celestin, S., Pasko, V.P., 2012. Source altitudes of terrestrial gamma-ray flashes produced by lightning leaders. Geophys. Res. Lett. 39, L08801. http://dx.doi.org/10.1029/2012GL051351.